

Control of oxygen vacancies and Ce^{+3} concentrations in doped ceria nanoparticles via the selection of lanthanide element

N. Shehata · K. Meehan ·
M. Hudait · N. Jain

Received: 11 April 2012 / Accepted: 30 August 2012
© Springer Science+Business Media B.V. 2012

Abstract The effect of lanthanides that have positive association energies with oxygen vacancies, such as samarium and neodymium, and the elements with negative association energies, such as holmium and erbium, on ionization state of cerium and, consequently, the oxygen vacancy concentration in doped ceria nanoparticles are investigated in this article. Structural and optical characterizations of the doped and undoped ceria nanoparticles, synthesized using chemical precipitation, are carried out using transmission electron microscopy, X-ray diffractometry, optical absorption spectroscopy, and fluorescence spectroscopy. It is deduced that the negative association energy dopants decrease the conversion of Ce^{+4} into Ce^{+3} and, hence, scavenge the oxygen vacancies, evidenced by the observed increase in the allowed direct bandgap, decrease in the integrated fluorescence intensity, and increased the size of doped nanoparticles. The opposite trends are obtained when the positive association dopants are used. It is concluded that the determining

factor as to whether a lanthanide dopant in ceria acts as a generator or scavenger of oxygen vacancies in ceria nanoparticles is the sign of the association energy between the element and the oxygen vacancies. The ability to tailor the ionization state of cerium and the oxygen vacancy concentration in ceria has applications in a broad range of fields, which include catalysis, biomedicine, electronics, and environmental sensing.

Keywords Ceria nanoparticles · Association · Lanthanides · Oxygen vacancies

Introduction

In the last few years, cerium oxide (ceria) nanoparticles have extensively been studied due to their potential uses in various applications in different fields, such as UV absorbers and filters (Tsunekawa et al. 2000), polishing media in micro-electronics, luminescent materials (Oh et al. 2011), neuroprotective agents in biological systems (Das et al. 2007), and as catalysts in the fuel cell technology (Steel and Heinzl 2001). Oxides with the cubic fluorite structure like ceria are known to be excellent solid electrolytes when they are doped with certain cations due to the reduction of the energy barrier for oxygen migration and the improvement of the ionic conductivity (Andersson et al. 2006). It is reported that doping ceria with trivalent elements changes the structural

N. Shehata (✉) · K. Meehan · M. Hudait · N. Jain
Bradley Department of Electrical and Computer
Engineering, Virginia Tech, 302 Whittemore (0111),
Blacksburg, VA 24061, USA
e-mail: nader83@vt.edu

N. Shehata
Department of Engineering Mathematics and Physics,
Faculty of Engineering, Alexandria University,
Alexandria, Egypt

properties of ceria. In general, doping ceria with trivalent elements results in a decrease in the lattice parameter as compared to undoped ceria, which is the result of an increased conversion process of Ce^{+4} ions to Ce^{+3} ions and a corresponding increase of the active oxygen vacancies (Deshpande et al. 2005). However, scandium, a trivalent element (Sc^{+3}), has been shown to produce an anomalous behavior in ceria where the dopant acts a scavenger for oxygen vacancies (V_O), pinning the vacancy in a $\text{Sc}-\text{V}_\text{O}$ pair, due to its negative association energy between vacancy and dopant (Gerhardt et al. 1987). Thus, not all trivalent element dopants cause an increased formation of active oxygen vacancies in ceria.

The control of oxygen vacancies in ceria will have a positive impact in many applications. For example, high- κ ceria films are currently deposited on germanium substrates to reduce the density of interface states in field effect transistor (FET). However, the Ge-based FETs suffer from leakage current since these films have relatively low bandgap and higher charge trapping (Chui et al. 2004). An increase in the ceria bandgap can be obtained by reducing the oxygen vacancy concentration, which will reduce charge trapping and, thus, the resulting degradation of the device performance. Another important application for ceria is gas sensing due to its oxygen storage capability, which is related to the concentration of oxygen vacancies (Elyassi et al. 2004). Ionic conductivity of thin film gas sensors is also dependent on the concentration of oxygen vacancies. The sensitivity and dynamic range of a ceria-based sensor can be maximized by optimizing the oxygen vacancy concentration. Also, an increase in oxygen vacancies can lead to improve the properties of ceria to act as free radical scavenger in biomedical applications (Babu et al. 2007). The increase of oxygen vacancies and ionic conductivity can be helpful in improving the catalytic activity of ceria for solid-state fuel cells applications (Zeng et al. 2010). As fluorescence efficiency of ceria is proportional to the percentage of cerium in the Ce^{+3} ionization state, the conversion of Ce^{+4} to Ce^{+3} determines the efficiency of ceria when used as a phosphorous material in solid-state lighting (Zholobak et al. 2011). One potential future application for ceria nanoparticles may be in bioimaging as the fluorescent wavelength of ceria is in the visible wavelength range (Shukla et al. 2004). Therefore, it is critical to control Ce^{+3} ionization states

and the corresponded concentration of oxygen vacancies for many applications.

In this study, the relationship among the vacancy-trivalent element association energies in doped ceria nanoparticles, synthesized using chemical precipitation, and the conversion of Ce^{+4} ions to Ce^{+3} ions is studied and correlated to the formation of active oxygen vacancies in ceria. The selected lanthanide elements are samarium, neodymium, holmium, and erbium. The first two elements have positive association energies, which may repel, or do not form complexes with oxygen vacancies, whereas the last two elements have relative negative V_O -dopant association energies. The negative sign indicates the trapping of oxygen vacancies (Andersson et al. 2006; Nakayama and Martin 2009; Wei et al. 2009). Optical and structural characterizations of doped ceria nanoparticles are performed to calculate the direct allowed bandgap, emitted fluorescent intensity, particle size, and lattice parameter as functions of dopant element and concentration. These characteristics are compared to those of the undoped ceria to determine whether there is a decrease or increase in the conversion process from Ce^{+4} to Ce^{+3} , a process which is correlated to an increase in the concentration of free oxygen vacancies.

Experimental procedure

There are many techniques that are used to produce doped ceria nanoparticles, including chemical precipitation (Suda et al. 2006), hydro-thermal synthesis (Dikmen et al. 1999), and solid-state reaction method (Yamamura et al. 2007). Compared to most methods, precipitation is attractive due to its use of inexpensive salt precursors, the simple process performed at room temperature and pressure, and the ease at which the process can be scaled for mass production (Dhannia et al. 2009). Therefore, this method is selected to synthesize the undoped ceria nanoparticles and the nanoparticles doped with the selected lanthanide elements (Sm, Nd, Ho, and Er).

Undoped ceria nanoparticles are prepared using a chemical precipitation technique similar to that described in Chen and Chang (2004). 0.5 g of cerium (III) chloride heptahydrate (99.9 %, Sigma-Aldrich) is added in 40-mL de-ionized (DI) water as a solvent. The solution is stirred constantly in an open container

at a rate of 500 rpm for 24 h while placing in a water bath. The water bath is heated to a temperature of 60 °C and held for approximately 1 min to ensure that the solution is homogeneous. 1.6 mL of ammonia is then added to the solution and the reaction is initiated immediately. The stirred solution is kept in a heated water bath for 1.5 h. In the second stage of the reaction, the solution is stirred for the remaining 22.5 h at room temperature.

The elevated temperature during the first stage of the synthesis process is important because it increases the conversion rate of $\text{Ce}(\text{OH})_3$, the first product of the reaction, to CeO_2 where cerium is in the Ce^{+4} ionization state. Then, CeO_2 is converted to Ce_2O_3 , where cerium exists as Ce^{+3} ions (Lawrence et al. 2011; Trovarelli 2005). Nonetheless, the initial reaction temperature is relatively low and the concentrations of reactants used are fairly dilute, relative to the synthesis parameters mentioned in Basu et al. (2004 and Guo 2007), to reduce the potential for agglomeration of the nanoparticles form in solution. The constant stirring of the solution assists in the fracturing of nanorods into nanoparticles.

The doped ceria nanoparticles are synthesized using the same procedure. However, the weight of cerium chloride and the doping element chloride depends on expected concentration of the rare earth (RE) element used as the dopant in the ceria nanoparticles. Thus, the quantities of the salts used in the synthesis of doped ceria nanoparticles are 0.025 g of RE chloride heptahydrate (RE = Sm, Nd, Ho, or Er) and 0.475 g of cerium chloride heptahydrate, 0.05 g of RE chloride heptahydrate and 0.45 g of cerium chloride heptahydrate, and 0.075 g of RE chloride heptahydrate and 0.425 g of cerium chloride heptahydrate to obtain a dopant weight ratio of 5, 10, and 15 %, respectively.

After the completion of the synthesis process, the colloidal solution is centrifuged and the centrifugate is washed with DI water and ethanol to remove any unreacted cerium and ammonia, and is then resuspended in DI water. This process is repeated for a second time, after the solution is sonicated to separate any agglomerates. Following these steps, the centrifugate is allowed to dry in air.

0.03 g of the dried powder then is suspended in 10 mL of DI water and sonicated prior to the fluorescence measurement. Approximately 3 mL of the colloidal solutions is pipetted into methacrylate cuvettes. The fluorescence spectroscopy system

consists of an ultraviolet (UV) lamp coupled to a monochromator (a 1/4 m Newport Cornerstone 260). The light that exits the monochromator ($\lambda_{\text{exc}} = 430$ nm) is focused on to the colloidal solution. The fluorescence signal is collected using a second monochromator (a 1/4 m Newport Cornerstone 260), positioned at an angle of 90° to the first monochromator. As monochromator is scanned over the visible wavelength region and the fluorescence signal is detected by the photomultiplier tube (Newport PMT 77340), located at the exit port of the second monochromator, and is measured using a power meter (Newport Power meter 2935C).

A further dilution of the samples by a factor of 4 is required when measuring the absorbance dispersion using dual-beam UV–vis–NIR spectrometer (UV-3101PC Shimadzu) to obtain data from 350 to 800 nm. The reference used during the absorption measurements is a methacrylate cuvette filled with DI water. The allowed direct bandgap can be calculated from the linear region of the absorbance dispersion curves, as will be discussed in “Results and discussion” section.

To determine the structure of the doped and undoped nanoparticles, the surface planes of different samples are measured using a PANalytical’s X’Pert PRO X-ray diffractometer (XRD) at 45 kV and 40 A with Cu K_α radiation ($\lambda = 0.154$ nm). The average diameter of the nanoparticles can be calculated from the first diffraction peak; the plane (111) of ceria. Images of the doped and undoped nanoparticles of the different samples are collected using transmission electron microscopy (TEM) (Philips EM420). The TEM samples are prepared by immersing carbon-copper mesh grids in colloidal solutions with the same concentration of nanoparticles used during the absorption measurements, which are then dried for 30 min before imaging. The average diameter of the nanoparticles is measured from the collected images and compared to the diameters calculated from XRD measurements. Also, the interplanar distance and the lattice parameter of the doped ceria nanoparticles can be calculated from the electron diffraction rings, which can be obtained during TEM imaging.

The concentrations of the chemical components of the synthesized nanoparticles are measured using a PHI Quantera SXM scanning X-ray photoelectron spectroscopy (XPS). Samples were prepared by drying colloidal solutions on quartz slides. Quantitative

analyses of the chemical elements and their chemical states found within the top few nanometers of a surface are performed. Concentration of the dopant elements in the nanoparticles is determined from the XPS data. Given that there is some ambiguity over the accuracy of the calculated ionization state of cerium, this technique was not used to quantify the concentration of Ce^{+4} and Ce^{+3} in the nanoparticle samples (Qiu et al. 2006), but is used as a qualitative confirmation of the trends determined from an analysis of the data collected using the other characterization equipment.

Results and discussions

The absorption dispersions for ceria doped with Nd and Er are presented in Fig. 1a, b as examples of the optical

absorption spectra collected on the colloidal nanoparticle solutions. For all samples, the absorbance dispersions have the same general shape, monotonically increasing with increasing photon energy, though they have slight difference in the magnitude and slope of the curves in the linear regions and the photon energy at which the nanoparticles begin to absorb strongly.

The relation among the absorption coefficient, the absorbed photon energy, and the allowed direct bandgap of the nanoparticles is described in Eq. (1) (Pankove 1971)

$$\alpha(E) = A(E - E_g)^{1/2} \quad (1)$$

where α is the absorbance coefficient, A is a constant that depends on the effective masses of electrons and holes in the material, E is the absorbed photon energy, and E_g is the allowed direct bandgap.

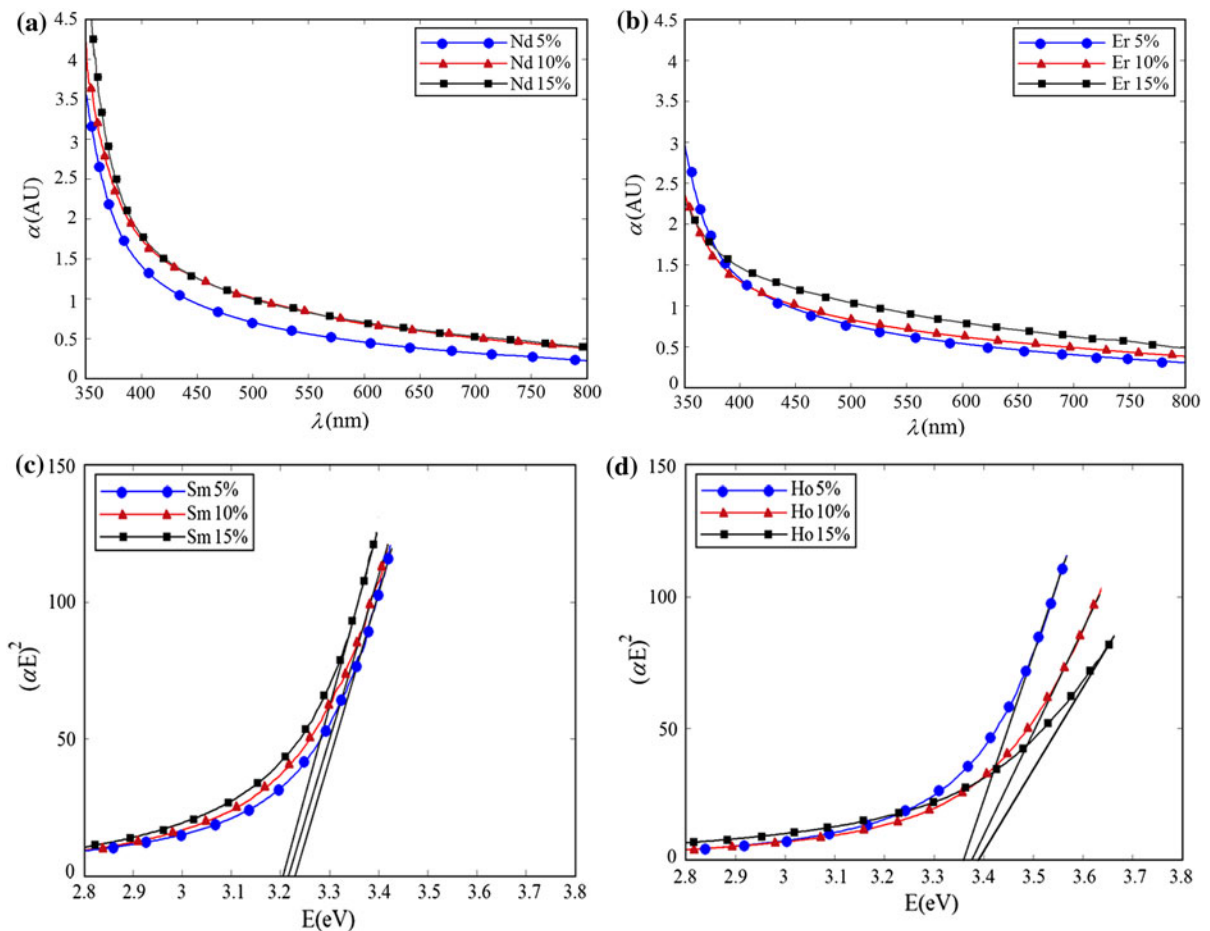


Fig. 1 Absorbance dispersion of ceria **a** doped with Nd, **b** doped with Er, and the direct bandgap calculations of ceria, **c** doped with Sm, and **d** doped with Ho

In Fig. 1c and d, $(\alpha E)^2$ versus E is plotted for samples doped with Sm and Ho, respectively. The intersection between the extrapolation of the linear portion of $(\alpha E)^2$ curve and x-axis is equal to the allowed direct bandgap of ceria nanoparticles. The bandgap of CeO_2 is roughly 4 eV while Ce^{+3} ions present in the crystal lattice, which could be considered a part of a Ce_2O_3 compound, create a trap state 3 eV above the CeO_2 valence band and correspond to the $\text{Ce}5d\text{--Ce}4f$ transition (Patsalas et al. 2003). Experimentally, the measured range of Ce_2O_3 bandgap is between 3.03 and 3.7 eV, depending on the synthesis method, reaction temperature, and the size of particles (Yin et al. 2002).

In this study, we have found that the bandgap of undoped ceria is 3.26 eV. We interpret that this is due to substantial concentration of Ce^{+3} ions in the undoped ceria nanoparticles produced via the chemical precipitation synthesis process described earlier. If the doped ceria nanoparticles are found to have a smaller bandgap than that found for the undoped ceria, then it is assumed that there are more Ce^{+3} states and a higher concentration of oxygen vacancies. However, if the value of bandgap for the doped ceria should be found to be greater than 3.26 eV, it is presumed that

more of the cerium is in the Ce^{+4} state and the concentration of V_O is smaller than that found in the undoped ceria samples.

From the calculations of E_g summarized in Table 1, it can be noted that the direct allowed bandgap of doped ceria is smaller than that of undoped ceria with the incorporation of dopants Sm or Nd, and the difference between the bandgap energy of the doped ceria and undoped ceria increases with increasing dopant concentration. This is also an evidence that there is a higher percentage of cerium in the Ce^{+3} state in the samples doped with Nd or Sm than in the undoped samples, which supports the hypothesis that ceria nanoparticles doped with a positive vacancy–dopant association energy trivalent element increase Ce^{+3} states and that leads to a higher concentration of V_O . Furthermore, the bandgap energies of nanoparticles doped with Ho and Er are larger than the bandgap of the undoped ceria and the magnitudes of direct bandgaps are larger with increasing the dopant concentration, an indication that the doping with negative vacancy–dopant association energy elements yields ceria nanoparticles with lower Ce^{+3} ionization states and lower V_O concentration than that the concentration that exists in the undoped ceria nanoparticles. In other words, the Sm and Nd act as

Table 1 Summary of the optical and structural properties of the undoped and RE-doped ceria samples (RE = Sm, Nd, Ho, and Er)

Material	Direct E_g (eV)	Peak fluorescence (norm.)	Lattice parameter (Å)	Interplanar distance (Å)	Mean particle size using TEM (nm)	Mean particle size using XRD (nm)
Undoped ceria	3.26	1	5.22	3.03	6.75	6.83
Doped with Sm						
5 %	3.24	1.10	5.27	3.04	6.29	6.30
10 %	3.23	1.21	5.31	3.07	6.23	6.29
15 %	3.21	1.33	5.35	3.09	6.21	6.10
Doped with Nd						
5 %	3.24	1.12	5.30	3.06	6.48	6.55
10 %	3.22	1.36	5.35	3.09	6.39	6.45
15 %	3.20	1.91	5.38	3.11	6.24	6.30
Doped with Ho						
5 %	3.36	0.86	5.09	2.94	7.21	7.12
10 %	3.38	0.70	4.99	2.88	7.25	7.31
15 %	3.39	0.67	4.94	2.85	7.33	7.44
Doped with Er						
5 %	3.32	0.98	5.08	2.93	7.36	7.12
10 %	3.33	0.82	5.04	2.91	7.48	7.44
15 %	3.34	0.78	5.01	2.89	7.60	7.79

oxygen vacancy generators and Er and Ho act as oxygen vacancy scavengers due to the increase and decrease of Ce^{+3} ionization states, respectively. The 4-eV bandgap of cerium dioxide is an indirect gap. Hence, there will be a very small probability that radiative recombination will occur when the Ce^{+4} ions in CeO_2 are optically excited. On the other hand, Ce_2O_3 has a direct bandgap of 3.26 eV, as mentioned before, and the relaxation via the $5d-4f$ transition of an excited Ce^{+3} ions in Ce_2O_3 , results in a photon emission (Patsalas et al. 2003). When ceria that contains some fraction of Ce_2O_3 is illuminated with UV light, the valence band electrons can easily be excited to an oxygen vacancy defect state located within the CeO_2 bandgap. From the V_O defect state, the electron undergoes multiple transitions before it returns to the ground state. Energy is radiatively released during one of the transitions; the emitted photon has a wavelength around 520 nm. The other transitions are non-radiative. Therefore, the rate at which photons are emitted from ceria via spontaneous emission, which is proportional to the peak intensity of the emitted fluorescence spectrum, is proportional to the number of electrons optically excited to the V_O defect state near the conduction band, corresponded to more Ce^{+3} ions. When there is a higher concentration of Ce^{+3} states and a corresponding high concentration of V_O states, a greater percentage of valence electrons can be excited to the defect state and a larger fluorescence signal will be emitted. In summary, a sample of ceria that has a strong fluorescence indicates that there is a higher

concentration of Ce^{+3} states in that sample as compared to a ceria sample that has a weak fluorescence signal. The fluorescence spectra for ceria doped with Sm and Er are shown in Fig. 2a and b, respectively. A summary of the peak fluorescence intensities, normalized to the undoped ceria fluorescent intensity for all of the doped and undoped ceria nanoparticles, is reported in Table 1. The peak fluorescence intensity is highest in the ceria samples doping with the two positive association energy elements, Sm and Nd, as compared to that of undoped ceria, which is an evidence that there are higher concentrations of Ce^{+3} ions and more active oxygen vacancies in these doped samples.

The opposite behavior is found within ceria samples doped with negative association energy dopants, Ho and Er, which is an indication that there is a reduction in the concentration of oxygen vacancies due to a lower percentage of cerium in the Ce^{+3} state. The conclusions drawn from the fluorescence data are in good agreement within the results obtained from the direct bandgap calculations.

TEM images of undoped and some of the doped ceria nanoparticles, associated with diffraction rings, are shown in Fig. 3. The average size, interplanar distances, and lattice parameters of the nanoparticles are calculated and reported in Table 1. From these results, it can be noted that the particle size becomes smaller and the interplanar distance and lattice parameter are increased when ceria is doped with a positive association energy element such as Sm and Nd, as compared to undoped ceria. These structural

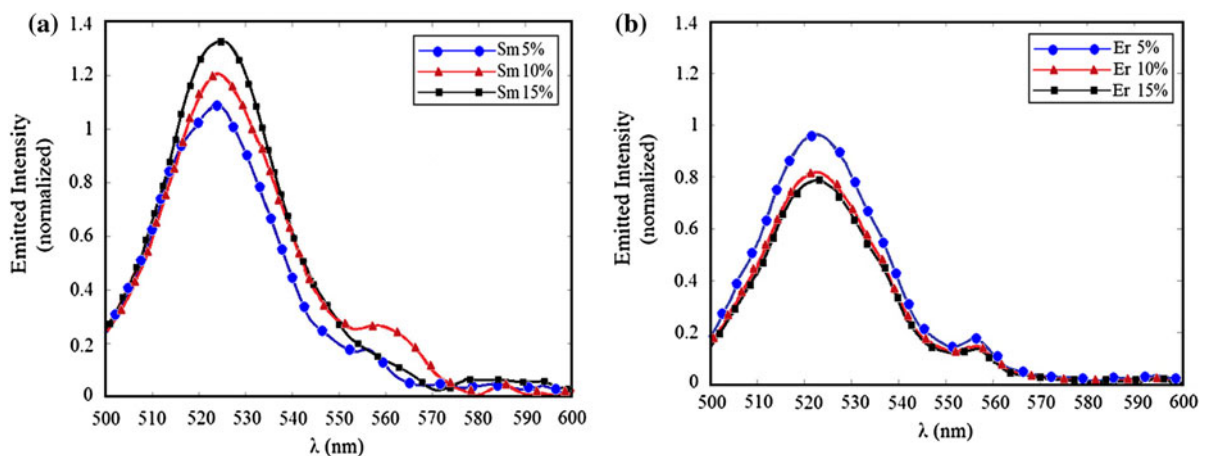


Fig. 2 Fluorescence emission from ceria doped with 5, 10, and 15 %, by reagent weight, of **a** Sm and **b** Er (All the emitted intensities are normalized to the undoped ceria fluorescence)

changes can result from the increased lattice strain that produced by high concentrations of the oxygen vacancies associated with Ce^{+3} ions in the doped ceria (Deshpande et al. 2005). The opposite trends in structural changes are found when the dopant is a negative association lanthanide such as Ho and Er. This provides further evidence that the ceria doped with positive association lanthanide dopants contain higher Ce^{+3} ionization states and concentration of oxygen vacancies and that the negative association lanthanide dopants reduce the concentration of oxygen vacancies in ceria nanoparticles related to lower Ce^{+3} ionization states.

X-ray diffractometer (XRD) patterns are presented in Fig. 4 for (a) undoped ceria and (b) ceria doped with 5 % Nd as examples. In Fig. 4b, the XRD pattern of the doped ceria nanoparticles demonstrates that the sample is composed of Nd-doped ceria as opposed to a mixture of neodymium oxide nanoparticles and ceria

nanoparticles. The same conclusion is derived from the other doped ceria XRD patterns.

The average diameter of the nanoparticles can be calculated from the angular position of the first pattern peak, which corresponds to the most stable surface plane, (111), among the low-index planes of ceria (Deshpande et al. 2005), using Scherrer's formula

$$d = \frac{0.9\lambda}{\beta \cos\theta}, \quad (2)$$

where d is the average diameter of the particles, λ is the wavelength of X-ray, β is the full width half maximum (FWHM) of the surface plane pattern, and θ is the diffraction angle. The average diameters for all of the undoped and doped ceria samples are reported in Table 1. The average particle size for each sample is in good agreement with the results obtained from the TEM images. This corroborates the conclusions drawn from the analysis of TEM images that the addition of a

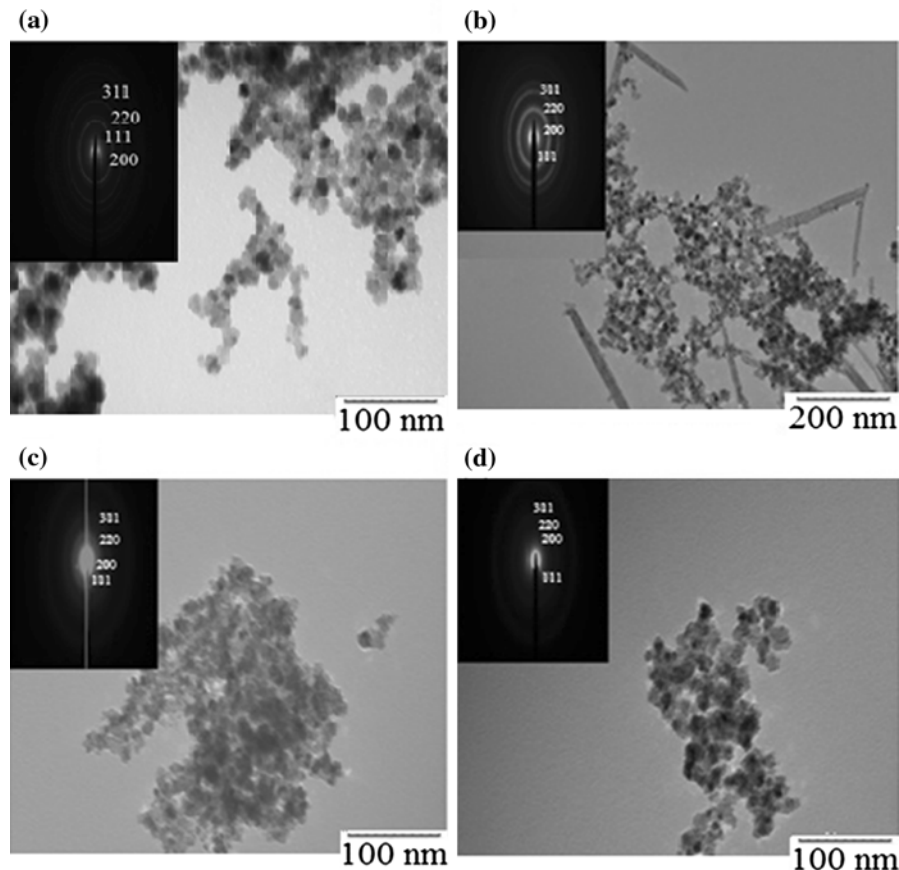
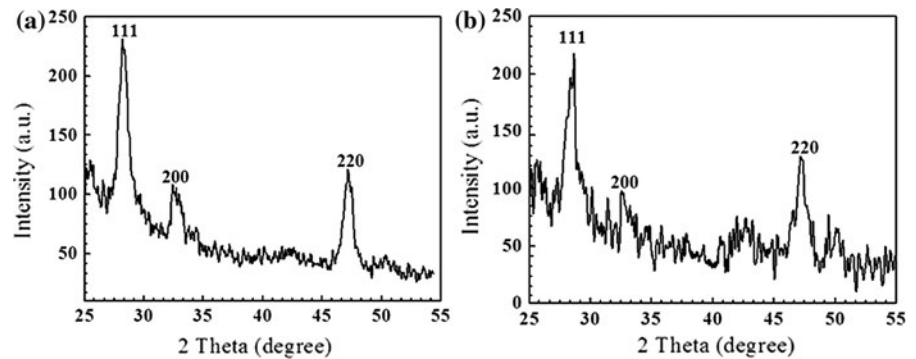


Fig. 3 TEM images and diffraction rings of ceria **a** undoped, **b** doped with 5 % Ho, **c** doped with 5 % Er, and **d** doped with 5 % Nd

Fig. 4 XRD patterns of ceria: **a** undoped and **b** doped with 5 % Nd as examples



lanthanide dopant with positive vacancy–dopant association energy generates more oxygen vacancies in ceria and that a lanthanide dopant with negative association energy reduces the concentration of oxygen vacancies in ceria nanoparticles as compared to the V_O concentration in undoped ceria.

Table 2 lists the results from the analysis of the doped ceria nanoparticles obtained from XPS and provides a quantitative overview of the chemical composition of each synthesized nanoparticles. It is observed that the incorporation of dopant in the ceria nanoparticles during synthesis was higher when the dopant has negative association energy. Several trends can be observed from the analysis of the data presented in the two tables. Of the two oxygen vacancies

generators, Nd causes a larger change in the oxygen vacancy concentration, compared to what obtained when an equal weight of Sm is added. In other words, there is a higher concentration of Ce^{+3} ions formed in the ceria doped with Nd more than the doped ceria with Sm. Ho is a much better vacancy scavenger than Er as there is a more significant reduction of Ce^{+3} states in the Ho-doped ceria, based upon the decreases in allowed direct bandgap and peak fluorescence intensity with increasing dopant concentration. The relationship between conversion rate from Ce^{+4} to Ce^{+3} states, or the corresponding oxygen vacancy concentration, and the amount of dopant in the ceria nanoparticles appears to be relatively linear when the dopant is either Nd or Sm, but is strongly nonlinear

Table 2 Chemical analysis of the atomic concentrations of synthesized nanoparticles

Weight ratios	O1s	Ce3d	Sm3d	Nd3d	Ho4d	Er4d	Molecular percentage of dopants
Undoped ceria	62.62	10.39	0	0	0	0	0
Doped with Sm							
5 %	62.10	12.34	0.76	0	0	0	6.16
10 %	65.63	12.14	1.09	0	0	0	8.98
15 %	65.40	10.13	1.73	0	0	0	17.08
Doped with Nd							
5 %	65.31	11.86	0	0.29	0	0	2.45
10 %	66.03	10.70	0.44	0	0	0	4.11
15 %	65.45	10.97	0	0.96	0	0	8.75
Doped with Ho							
5 %	66.68	12.03	0	0	0.38	0	3.16
10 %	67.02	8.01	0	0	1.02	0	12.6
15 %	68.30	10.99	0	0	1.44	0	13.10
Doped with Er							
5 %	69.77	10.61	0	0	0	0.46	4.34
10 %	60.02	14.31	0	0	0	1.34	10.68
15 %	69.36	8.17	0	0	0	1.85	22.64

when the dopant is Ho or Er. The largest changes in the properties of the doped ceria nanoparticles occur when the dopant concentration is roughly below 5 % for either of these two dopants.

Conclusion

It can be concluded that not all trivalent lanthanide elements, used as dopants in ceria nanoparticles, increase the conversion of cerium from Ce^{+4} to Ce^{+3} or increase the oxygen vacancy concentration. This fact is first noted in the past for scandia-doped bulk ceria. A correlation between association energy of the lanthanide dopant element and its ability to increase or decrease the conversion of Ce^{+4} to Ce^{+3} and enhance or suppress the formation of oxygen vacancies in ceria nanoparticles is demonstrated in this study. The lanthanide dopants with positive association energies, such as samarium and neodymium, increase the conversion rate from Ce^{+4} ionization state to Ce^{+3} state and consequently increase the oxygen vacancies in ceria nanoparticles. However, lanthanide elements with negative association energies, such as holmium and erbium, reduce the percentage of cerium that exists in the Ce^{+3} ionization states and scavenge oxygen vacancies in the synthesized ceria nanoparticles.

There are major findings presented in this study that demonstrate this conclusion. First, the ceria nanoparticles doped with one of the positive association dopants had a smaller direct bandgap as compared to undoped ceria. Second, the integrated emitted fluorescent intensity of the ceria doped with a lanthanide with positive association energy was higher relative to that of undoped ceria sample. The next piece of evidence is that the average diameter of the nanoparticles doped with a lanthanide with positive association energy is smaller and the lattice parameter and interplanar distance are larger than that found for undoped ceria. The opposite trends in material properties are found when the dopant is a lanthanide with negative association energy.

The results of this study suggest that the concentrations of Ce^{+3} ionization states and the corresponded oxygen vacancies in ceria nanoparticles can be controlled by selecting the lanthanide element with the appropriate vacancy–dopant association energy and its concentration during the ceria nanoparticle synthesis process. This novel concept to engineer the generation

or scavenging the oxygen vacancies and to determine the dominant Ce ionization states via the selection of lanthanide dopant and dopant concentration can have significant impact in a range of applications that include high mobility Ge FETs, gas sensors, solid-state phosphors, and nano-biomedical therapeutic agents.

Acknowledgments This study was funded in part by a NSF STTR Phase I grant with MW Photonics (award# 0930364). Shehata was funded through Virginia Tech Middle East and North Africa (VT-MENA) program. The authors thank Dr. Niven Monsegue, Dr. Jerry Hunter, and Andrew Giordani from the Nanotechnology Characterization and Fabrication Laboratory, Institute of Critical Technologies and Applied Science at Virginia Tech for their training and assistance with the TEM and XPS measurements. Also, the authors appreciate the support of Mr. Don Leber, manager of the Micron Technology Semiconductor Processing Laboratory at Virginia Tech.

References

- Andersson DA, Simak SI, Skorodumova NV, Abrikosov IA, Johansson B (2006) Optimization of ionic conductivity in doped ceria. *Proc Natl Acad Sci USA* 83:1–4. doi: [10.1073/pnas.0509537103](https://doi.org/10.1073/pnas.0509537103)
- Babu S, Velez A, Wozniak K, Szydłowska J, Seal S (2007) Electron paramagnetic study on radical scavenging properties of ceria nano-particles. *Chem Phys Lett* 442:405–408
- Basu S, Devi PS, Maiti HS (2004) Synthesis and properties of nanocrystalline ceria powders. *J Mater Res* 19(11): 3162–3171. doi: [10.1557/JMR.2004.0442](https://doi.org/10.1557/JMR.2004.0442)
- Chen H, Chang H (2004) Homogeneous precipitation of cerium dioxide nanoparticles in alcohol/water mixed solvents. *Colloid Surf A* 242:61–69. doi: [10.1016/j.colsurfa.2004.04.056](https://doi.org/10.1016/j.colsurfa.2004.04.056)
- Chui CO, Kim H, McIntyre PC, Saraswat KC (2004) Atomic layer deposition of high- κ dielectric for germanium MOS applications—substrate surface preparation. *IEEE Elect Device Lett* 25(5):274–276
- Das M, Patil S, Bhargava N, Kang JF, Riedel LM, Seal S, Hickman JJ (2007) Auto-catalytic ceria nanoparticles offer neuro-protection to adult rat spinal cord neurons. *Biomaterials* 28:1918–1925
- Deshpande S, Patil S, Kuchibhatla S, Seal S (2005) Size dependency variation in lattice parameter and valency states in nanocrystalline cerium oxide. *Appl Phys Lett* 87: 133113. doi: [10.1063/1.2061873](https://doi.org/10.1063/1.2061873)
- Dhannia T, Jayalekshmi S, Kumar MCS, Rao TP, Bose AC (2009) Effect of aluminum doping and annealing on structural and optical properties of cerium oxide nanocrystals. *J Phys Chem Solids* 70:1443–1447. doi: [10.1016/j.jpcs.2009.09.001](https://doi.org/10.1016/j.jpcs.2009.09.001)
- Dikmen S, Shuk P, Greenblatt M (1999) Hydrothermal synthesis and properties of $Ce_{1-x}La_xO_2$ solid solutions. *Solid State Ion* 126:89–95

- Elyassi B, Rajabbeigi N, Khodadadi A, Mohajerzadeh SS, Sahimi M (2004) An yttria-doped ceria-based oxygen sensor with solid-state reference. *Orig Res Art Sens Act B* 103(1):178–183
- Gerhardt R, Lee WK, Nowick AS (1987) Anelastic and dielectric relaxation of scandia-doped ceria. *J Phys Chem Solids* 48(6):563–569. doi:0022/369718
- Guo H (2007) Green and red upconversion luminescence in $\text{CeO}_2:\text{Er}^{+3}$ powders produced by 785 nm laser. *J Solid State Chem* 180:127–131. doi:10.1016/j.jssc.2006.10.003
- Lawrence NJ, Jiang K, Cheung CL (2011) Formation of a porous cerium oxide membrane by anodization. *Chem Commun* 47:2703–2705
- Nakayama M, Martin M (2009) First-principles study on defect chemistry and migration of oxide ions in ceria doped with rare-earth cations. *Phys Chem Chem Phys* 11:3241–3249
- Oh M, Nho J, Cho S, Lee J, Sing R (2011) Polishing behaviours of ceria abrasives on silicon dioxide and silicon nitride. *CMP J Powder Tech* 206:239–245
- Pankove J (1971) *Optical processes in semiconductors*. Dover Publications Inc., New York
- Patsalas P, Logothetidis S, Sygellou L, Kennou S (2003) Structure-dependent electronic properties of nanocrystalline cerium oxide films. *Phys Rev B* 68(3):035104–035117
- Qiu L, Liu F, Zhao L, Ma Y, Ya J (2006) Comparative XPS study of surface reduction for nanocrystalline and microcrystalline ceria powder. *Appl Surf Sci* 25:4931–4935
- Shukla A, Mukherjee S, Sharma S, Agrawal V, Kishan K, Guptasarma P (2004) A novel UV laser-induced visible blue radiation from protein crystals and aggregates: scattering artifacts or fluorescence transitions of peptide electrons delocalized through hydrogen bonding. *Arch Biochem Biophys* 428(2):144–153
- Steel B, Heinzl B (2001) Materials for fuel-cell technologies. *Nature* 414:345–352
- Suda E, Pacaud B, Mori M (2006) Sintering characteristics, electrical conductivity and thermal properties of La-doped ceria powders. *J All Comp* 408:1161–1164
- Trovarelli A (2005) *Catalysis by ceria and related materials*, 2nd edn. Imperial College Press, London
- Tsunekawa S, Fukuda T, Kasuya A (2000) Blue shift in ultraviolet absorption spectra of monodisperse CeO_{2-x} nanoparticles. *J Appl Phys* 87(3):1318–1321
- Wei X, Pan W, Cheng L, Li B (2009) Atomistic calculation of association energy in doped ceria. *Solid State Ion* 180:13–17
- Yamamura H, Takeda S, Kakinuma K (2007) Dielectric relaxations in the $\text{Ce}_{1-x}\text{Nd}_x\text{O}_2$. *Solid State Ion* 178:1059–1064
- Yin L, Wang Y, Pang G, Koltypin Y, Gedanken A (2002) Sonochemical synthesis of cerium oxide nanoparticles—effect of additives and quantum size effect. *J Colloid Interface Sci* 246:78–84
- Zeng S, Wang L, Gong M, Chen Y (2010) Catalytic properties of Ni/ceria–yttria electrode materials for partial oxidation of methane. *J Nat Gas Chem* 19:509–514
- Zholobak NM, Ivanov VK, Shcherbakov AB, Shaporev AS, Polezhaeva OS, Baranchikov AY, Spivak NY, Tretyakov YD (2011) UV-shielding property, photocatalytic activity and photocytotoxicity ceria colloid solutions. *J Photochem Photobiol B* 102:32–38